Journal Homepage: -www.journalijar.com

INTERNATIONAL JOURNAL OF ADVANCED RESEARCH (IJAR)

Article DOI:10.21474/IJAR01/12044
DOI URL: http://dx.doi.org/10.21474/IJAR01/12044

RESEARCH ARTICLE

DIRECT TORQUE CONTROL OF A CENTRIFUGAL PUMP POWERED BY A PHOTOVOLTAIC SYSTEM WITH MPPT

Alkassoum Nabil[1], Boureima Seibou[2], Ousman Mahamadou Nabourkou[2], AssaridIssaka Abdoulkarim[3], Mamane Adamou[1], André Foulani[1] and Amadou Seidou Maiga[4]

1. Laboratoire d'Automatique, d'Electronique, d'Electrotechnique et d'Informatique Industrielle et d'Energie Renouvelable (LA2EI-ER), University Abdou Moumouni (Niamey).
2. School of Mines, of Industry and Geology (Niamey).
3. Physics Department, University Abdou Moumouni (Niamey).
4. Laboratoire d'Electronique, Informatique Télécommunications et d'Energies Renouvelables (LEITER), Gaston Berger University, Saint-Louis, Senegal.

Manuscript Info

Manuscript History
Received: 10 September 2020
Final Accepted: 15 October 2020
Published: November 2020

Key words:-
Photovoltaic Generator, MPPT, PWM Inverter, DTC, Induction Motor, Centrifugal Pump

Abstract

Water pumping is a very important operation in the agricultural and industrial fields. Due to its arid nature, our Saharan environment has a significant solar energy resource that allows the installation of water pumping systems using photovoltaic solar pumps. For this type of system, and to improve its performance, a prior theoretical study is necessary. Given the intermittent and fluctuating nature of the solar resource, it is essential to set up a system that allows its optimal exploitation. The aim of this work is to describe, develop and simulate a direct control of the DTC torque of a solar pumping system with optimised efficiency. The system consists of a three-phase asynchronous motor, coupled to a centrifugal pump, powered by a photovoltaic generator. The operation of the photovoltaic generator will be ensured at its maximum power via the MPPT control of a BOOST converter. Two control strategies for the motor pump were implemented and compared.The first, based on a sinus-delta MPPT control of the three-phase inverter supplying the motor pump. The second,uses direct torque control DTC to control the operation of the induction motor driving the centrifugal pump. The DTC control technology will be further developed. A dynamic model of the motor driving the pump will be shown. The performance provided by the introduction of DTC control will be presented. In addition, a control system will be established in this work, which allows the set speed of the asynchronous machine and thus the pump output to be set according to the state of sunlight. The complete model of the established system will be implemented and simulated in the simulation environment of the MATLAB software.

Copy Right, IJAR, 2020,. All rights reserved.

Corresponding Author:- Alkassoum Nabil
Address:- Laboratoire d'Automatique, d'Electronique, d'Electrotechnique et d'Informatique Industrielle et d'Energie Renouvelable (LA2EI-ER), University Abdou Moumouni (Niamey).

……

Introduction:-

Almost all of the energy sources used by humanity are provided by the sun. Every day, the Earth receives from the sun, through its radiation, the equivalent of several thousand times the total energy consumption of humanity for its activities. [04].

Solar energy is widely used to power isolated or desert regions. The great advantage is that this source is inexhaustible on a human scale, it is also very safe to use and is clean compared to other energy sources [01] [02].

It is particularly well suited for pumping water in rural areas [08] and on remote sites where access to conventional energy is difficult or almost impossible.Although not completely free, solar energy has low running costs and in some cases offers an economically viable alternative to conventional sources [00] [30].

For several decades, the DC motor and then the BLDC brushless motor have been used in pump systems as an electric actuator to drive the pump. Cost and maintenance issues led to research into the use of the squirrel cage induction motor as a new alternative.

Technological developments, particularly in the field of semiconductors, now make it possible to build high-power static converters capable of delivering voltages (currents) of adjustable amplitude and frequency. The increased possibilities of the control circuits allow the use of complicated mathematical operators; this is essential in order to regain, with AC machines, the flexibility of control and the quality of electromechanical conversion, naturally obtained until now with DC machines.

In this article, a technique for "optimising a solar photovoltaic pumping system" is modelled and simulated. The pumping system consists of an electronic chopper/three-phase inverter unit and an asynchronous motor unit-submerged centrifugal pump.

The optimisation consists of improving the machine's efficiency by introducing a direct torque control, DTC, adapted to the motor. It also consists of adding a BOOST converter with MPPT control at the output of the photovoltaic group in order to consume the maximum amount of energy available at its output. A comparative study of the simulation results of the optimised system and the system operating with the inverter connected directly to the group is carried out.

In what follows, a presentation of a conventional photovoltaic system will be made and the theoretical aspects relating to the said system will be discussed. Then a model of the photovoltaic system will be made and the results of the simulation will be presented. Finally an analysis of the results will be made.

Methodology:-

Our solar water pumping system consists of two basic components. On the surface there is a solar energy source which is conditioned and then transmitted via an electrical circuit at the bottom of the well to a submersible pump unit.

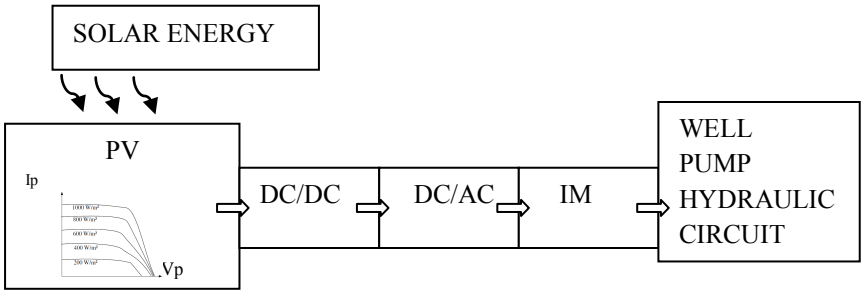

Figure 1:- Pumping system coupled directly to the solar source.

The simulation will require the elaboration of the mathematical model of each block of the system and of the global device.

Modelling the photovoltaic generator:
Photovoltaic (PV) panels generate the system's electrical energy. The smallest component of a PV panel is the solar cell (battery) that produces direct current (DC) electricity when exposed to light.

In the literature [03], [04], [13], [14], [18] [19] , the actual PV cell is most commonly modelled by an equivalent electrical circuit (see Figure 2) consisting of :

- an electric current generator shunted by a D-diode and an rsh resistor, to characterise the various leakage currents due to the diode and junction edge effects ;

- a series resistor rs representing the various contact and connection resistances.

There is also a double diode model including an additional diode for better curve fitting. Both models are implicit and non-linear [15].

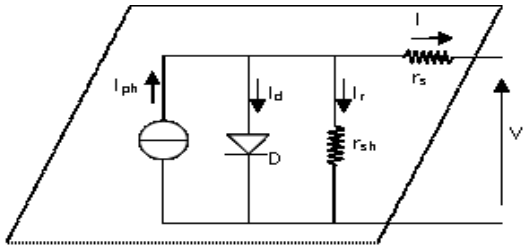

Figure 2:- Equivalent circuit of a photovoltaic cell.

By considering the equivalent scheme in Figure 2, one can determine the current of the photopile which is :

$$\mathbf{I = I_{ph} - I_0\left(e^{\frac{V+r_sI}{aV_T}} - 1\right) - \frac{V+r_sI}{r_{sh}}} \qquad \mathbf{(01)}$$

With ψ solar radiation..

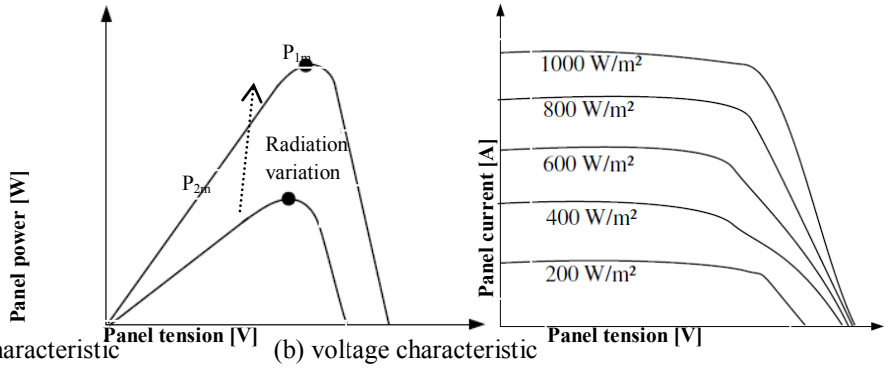

(a) power characteristic (b) voltage characteristic

Figure 3:- Typical characteristics of photovoltaic panels.

The current-voltage (I-V) characteristic of the photovoltaic cell in Figure 3 is non-linear. It describes the behaviour of the photovoltaic cell under specific sunlight and temperature conditions.

The resulting Simulink model is shown in Figure 4 as follows:

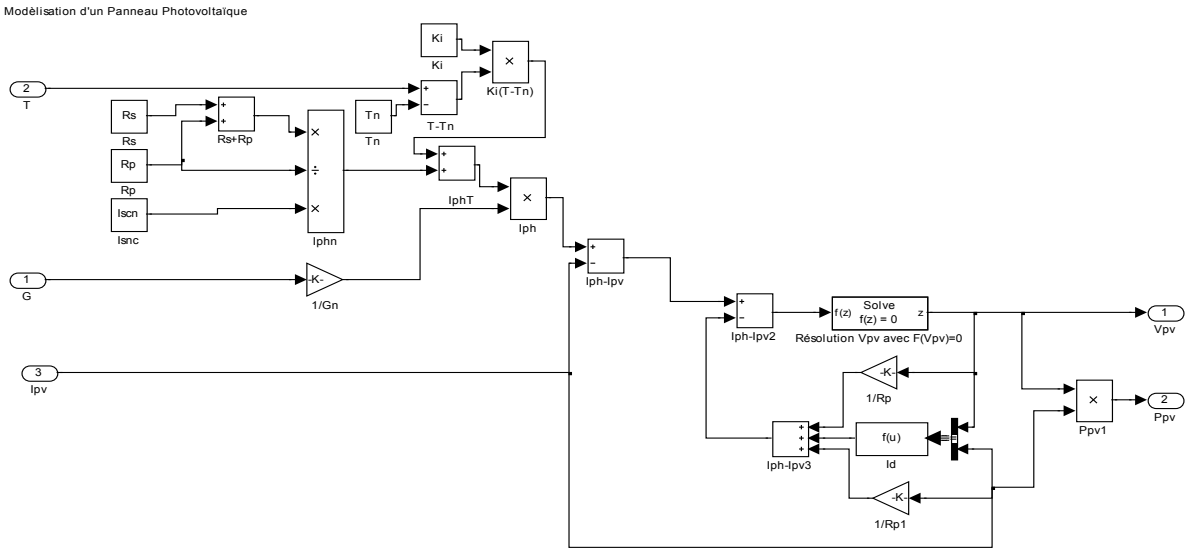

Figure 4:- Photovoltaic Panel Model with Matlab / Simulink.

Our model is based on the model shown in Figure 2, equation 01 of which describes the behaviour of an illuminated semiconductor junction, and on the classical approximations by various types of functions which can be carried out by taking into account the serial-parallel association of these junctions and the resistances introduced by the interconnections and welds. [16] [17] [04].

This model has a total of four variables, two input and two output variables.

Vpv: the voltage supplied by the panel;

The two input variables are : ψ : the illuminance on the panel (Wp or W/m^2); ;

T_j : the temperature of the panel junction (°C);

The two output variables are : I_{pv} : the current supplied by the panel;

V_{pv} : the voltage supplied by the panel ;

MPPT model:

The pump motor will hardly ever run at the maximum power point (Pmax) of the Photovoltaic generator during the day. In order to significantly improve this efficiency, the photovoltaic generator will be charged by an electronic system that will allow the electrical operating point of the modules to be varied so that they deliver the maximum available power. The electronic system enabling this function to be performed is the Maximum Power Point Tracking (MPPT) system, frequently referred to as MPPT (Power Point Tracking). [05] [04].

They are composed of a power circuit and a control circuit implementing an MPP maximum power point tracker algorithm. As shown in Figure 5, at the DC/DC converter input is the PV row and at the output is the load [06] [08] [04].

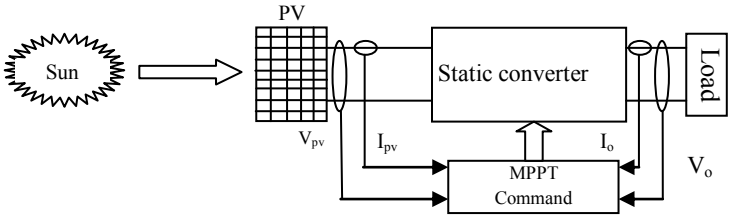

Figure 5:- Elementary photovoltaic conversion chain controlled by an MPPT.

The Boost converter is more suitable for photovoltaic systems with Maximum Power Point Tracking (MPPT) since the converter operates in direct current mode extracting as much power as possible from the solar cells. Therefore the energy efficiency of the Boost converter can be very high compared to other converters [04].

Model of the BOOST converter:
A basic diagram of the boost converter is given in figure 6 [04].

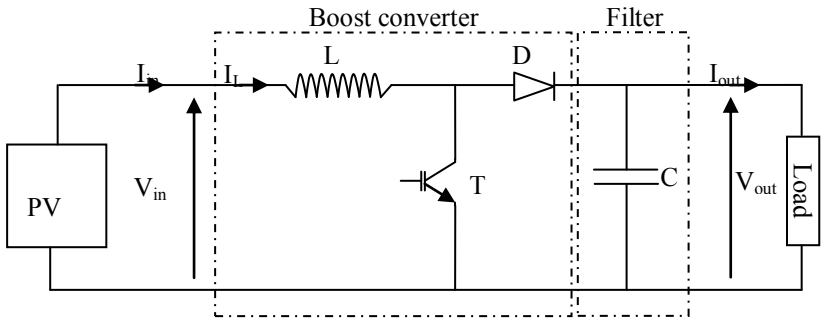

Figure 6:- Boost converter.

For reasons of simplification, we make the following assumptions: All elements are ideal; and The switching time is much shorter than the electrical time constant of the circuit, so a linear approximation can be used.

When switch T is closed during ton, diode D is reverse-biased by capacitance C and the power source (row of solar cells) thereby charging inductor L induces a current through it. At the same time, the load (inverter and induction motor) receives its power from the capacitor C. So we have :

$$\mathbf{V_{out} = V_C = \frac{1}{C}\int_0^{t_{on}} -I_{out}\, dt} \qquad (02)$$

$$\mathbf{I_{in} = I_L = \frac{1}{L}\int_0^{t_{on}} V_{in}\, dt} \qquad (03)$$

When T is open during toff, current flows from the power source through the inductor L and the diode D to recharge the output capacitor and simultaneously supply power to the load. We have therefore :

$$\mathbf{V_{out} = V_C = \frac{1}{C}\int_0^{t_{off}} (I_L - I_{out})\, dt} \qquad (04)$$

$$\mathbf{I_{in} = I_L = \frac{1}{L}\int_0^{t_{off}} (V_{in} - V_{out})\, dt} \qquad (05)$$

The Simulink model derived from these 4 equations is given in Figure 7 below :

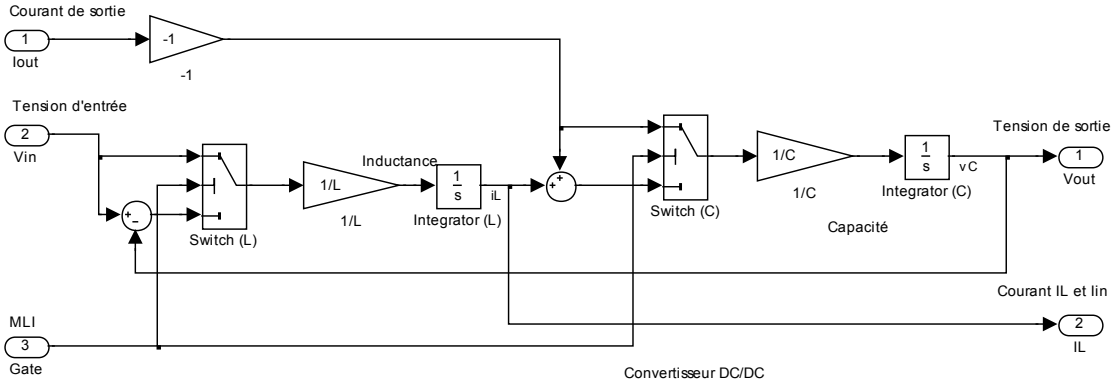

Figure 7:- Simulink model of the boost converter.

MPPT control model:

The basis of MPPT is to find a control strategy that gives the best ratio of the chopper switch control cycle so that the operating point on the PV Generator coincides with the maximum MPP power point.

There are two main categories of control strategy for the MPPT system, those with indirect algorithms (Quasi-tracker) and those with direct algorithms (True-tracker) [21].

One of the most widely used techniques in the literature [04], [21] dealing with the implementation of an MPPT in a photovoltaic system is that of "disturbance and observation".

It is this technique that we propose to implement in our system.

This technique is available in several variants for its implementation. It consists of calculating the MPP by iteration. It measures the PPV power on the panels,then perturbs the operating point to detect the power variation. If the power increases, the system continues in this direction, but if it decreases the direction of the disturbance is reversed. When the MPP is reached the system will oscillate around the maximum measured PPV power. s small, the disturbance that will be injected must be relatively very small. The algorithm for this technique is given in Figure 8.

D :duty cycle and
ΔD : perturbation

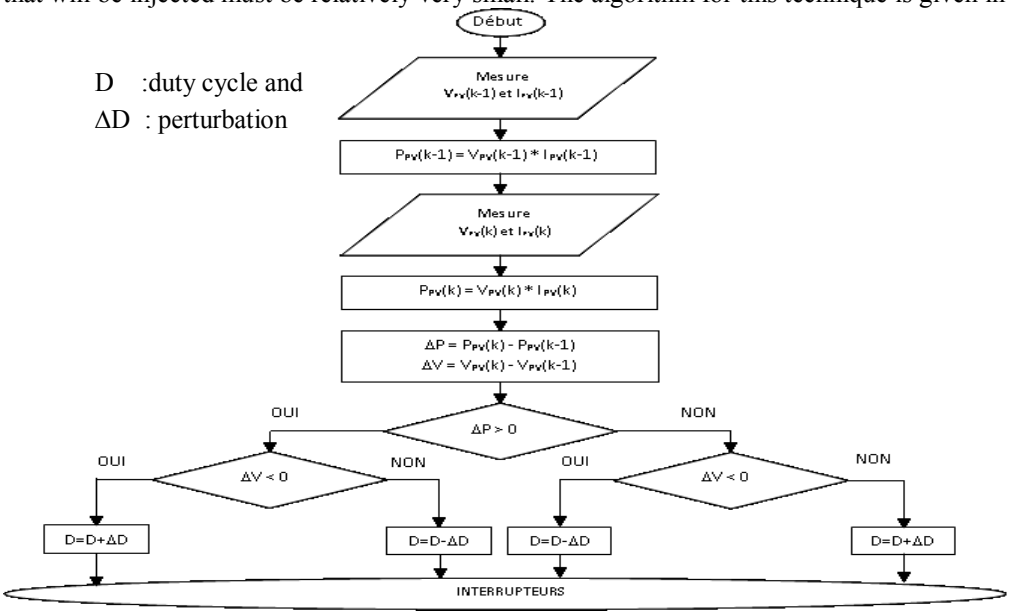

Figure 8:- « Perturbation and Observation » Algorithm

His model in Simulink is as follows:

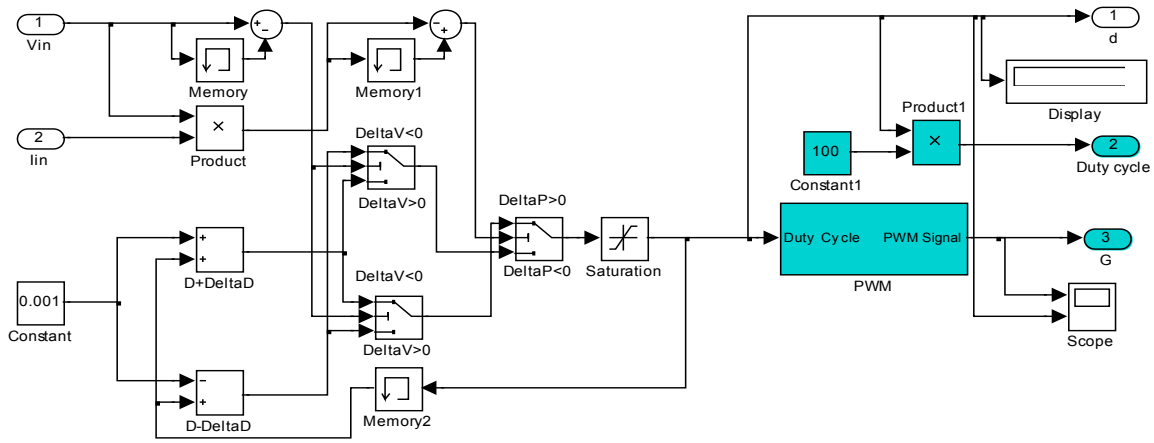

Figure 9:- Simulink Model of the Algorithm « Perturbation and Observation »

Model of the inverter:

The inverter is used to convert a direct current (DC) voltage into an alternating current (AC) voltage. Figure 10 shows a schematic diagram of the DC-AC conversion stage under a three-phase assumption.

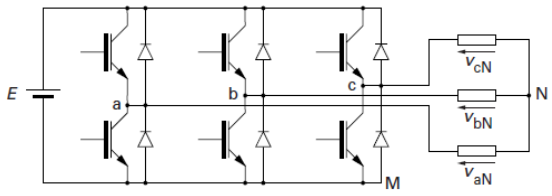

Figure 10:- Schematic diagram of an AC machine power inverter.

In this type of inverter, the chopped voltages are applied directly to the machine, of which inevitably the switching inductances of the latter act as current filters, provided that the chopping frequency used is adapted to the values of these inductances (pulse width modulation).

The inverter generates a three-phase voltage system, variable in amplitude and frequency, which operates with variable loads. If each cell is assigned a modulation function f_{ca}, f_{cb} and f_{cc} respectively, and the control is complementary on the same cell, the phase voltage can be expressed as follows [04] [07] :

$$\begin{bmatrix} V_{aN} \\ V_{bN} \\ V_{cN} \end{bmatrix} = \frac{V_{pv}}{3} \begin{bmatrix} 2 & -1 & -1 \\ -1 & 2 & -1 \\ -1 & -1 & 2 \end{bmatrix} \begin{bmatrix} f_{ca} \\ f_{cb} \\ f_{cc} \end{bmatrix} \quad (05)$$

As a matter of principle, this inverter operates discreetly. It can only take 23 = 8 states.

With the help of the above relationships, a list of these states and their associated voltages can be drawn up (Table 1).

Table 1:- States of a three-phase inverter.

States of the modulation functions			Neutral voltage	Three-phase single voltages		
f_{ca}	f_{cb}	f_{cc}	V_{NM}	V_{aN}	V_{bN}	V_{cN}
0	0	0	0	0	0	0
1	0	0	$V_{pv}/3$	$2\ V_{pv}/3$	$-\ V_{pv}/3$	$-\ V_{pv}/3$
1	1	0	$2\ V_{pv}/3$	$V_{pv}/3$	$V_{pv}/3$	$-2\ V_{pv}/3$
0	1	0	$V_{pv}/3$	$-\ V_{pv}/3$	$2\ V_{pv}/3$	$-\ V_{pv}/3$
0	1	1	$2\ V_{pv}/3$	$-2\ V_{pv}/3$	$V_{pv}/3$	$V_{pv}/3$
0	0	1	$V_{pv}/3$	$-\ V_{pv}/3$	$-\ V_{pv}/3$	$2\ V_{pv}/3$
1	0	1	$2\ V_{pv}/3$	$V_{pv}/3$	$-\ V_{pv}/3$	$V_{pv}/3$
1	1	1	0	0	0	0

Modeling the inverter in Simulink given in Figure 11 will use equation 56.

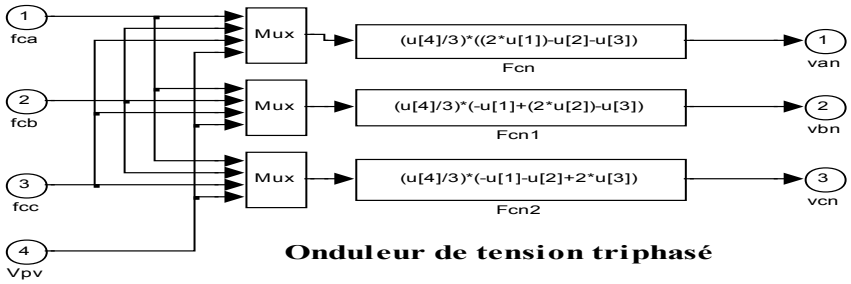

Figure 11:- Simulink model of the inverter.

Model of the moto pump unit:

Motor model:

In order to "better" control or regulate an asynchronous motor, it is essential to establish a model that is as close as possible to the behaviour of the machine to be controlled.

In what follows, we will try to formalise a relatively simplified model by posing (realistic) hypotheses generally used [09] [11] in this context :

Hypothesis:
The hypothesis generally accepted in the asynchronous machine model are:
1. the absence of saturation and losses in the magnetic circuit (hysteresis and eddy currents are negligible);
2. The perfect symmetry of the machine;
3. The sinusoidal spatial distribution of the different magnetic fields along the air gap. (The air gap is constant) ;
4. The equivalence of the short-circuited rotor to a three-phase star-connected winding;
5. Power is supplied by a symmetrical three-phase voltage system;
6. The winding resistances do not vary with temperature and the skin effect is neglected;

Thus, among the important consequences of these assumptions are the following:
1. The constancy of the own inductances;
2. The constancy of the stator and rotor resistances;
3. The law of sinusoidal variation of the mutual inductances between the stator and rotor windings as a function of the angle of their magnetic axes.

The following figure 12 gives a schematic representation of such an induction motor in the case of a single pole pair.

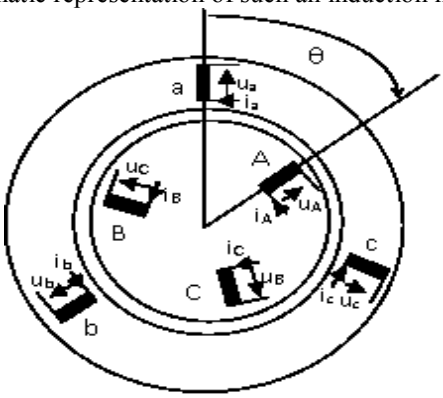

Figure 12:- Schematic representation of an asynchronous motor (p=1).

The stator phases are represented by windings a, b, c; the rotor phases by windings A, B, C. The angle represents the angle between the magnetic axis of the stator phase a and the magnetic axis of the rotor phase A. It therefore defines the position of the rotor in relation to the stator. The speed = d/dt is then the rotational speed of the motor, if the motor has only one pair of poles (if the motor has p pairs of poles, the rotational speed = / p).

We therefore have to define five inductances:
1. L_{aa} : inductance of a stator phase; ;
2. L_{AA} : self-inductance of a rotor phase ;
3. L_{ab} : mutual inductance between stator phases ;
4. L_{AB} : mutual inductance between rotor phases ;
5. $L_{aA}(\theta)$: mutual inductance between stator and rotor phases.

The fluxes through the windings are given in a matrix form by the following relationships:

$$[\psi_{abc}] = [L_s][i_{abc}] + [L_{sr}][i_{ABC}] \quad (1)$$
$$[\psi_{ABC}] = [L_r][i_{ABC}] + [L_{sr}][i_{abc}] \quad (2) \qquad (06)$$

Where :

$$[\psi_{abc}] = [\psi_a \psi_b \psi_c]^T \qquad [\psi_{ABC}] = [\psi_A \psi_B \psi_C]^T$$
$$[i_{abc}] = [i_a i_b i_c]^T \qquad [i_{ABC}] = [i_A i_B i_C]^T$$
$$[L_s] = \begin{bmatrix} L_{aa} & L_{ab} & L_{ab} \\ L_{ab} & L_{aa} & L_{ab} \\ L_{ab} & L_{ab} & L_{aa} \end{bmatrix} \qquad [L_r] = \begin{bmatrix} L_{AA} & L_{AB} & L_{AB} \\ L_{AB} & L_{AA} & L_{AB} \\ L_{AB} & L_{AB} & L_{AA} \end{bmatrix}$$

$$[L_{sr}] = [L_{aA}]\begin{bmatrix} \cos(\theta) & \cos(\theta+\frac{2\pi}{3}) & \cos(\theta-\frac{2\pi}{3}) \\ \cos(\theta-\frac{2\pi}{3}) & \cos(\theta) & \cos(\theta+\frac{2\pi}{3}) \\ \cos(\theta+\frac{2\pi}{3}) & \cos(\theta-\frac{2\pi}{3}) & \cos(\theta) \end{bmatrix}$$

Les équations de tension s'écrivent, sous leur forme matricielle comme suit :

$$[\mathbf{u_{abc}}] = [\mathbf{R_s}][\mathbf{i_{abc}}] + \frac{\mathbf{d}}{\mathbf{dt}}[\psi_{\mathbf{abc}}] \quad (1)$$

$$[\mathbf{u_{ABC}}] = [\mathbf{R_r}][\mathbf{i_{ABC}}] + \frac{\mathbf{d}}{\mathbf{dt}}[\psi_{\mathbf{ABC}}] \quad (2) \qquad (07)$$

Where :

$[u_{abc}] = [u_a u_b u_c]^T$ $\qquad [\psi_{ABC}] = [u_A u_B u_C]^T$

$$[R_s] = \begin{bmatrix} R_a & 0 & 0 \\ 0 & R_a & 0 \\ 0 & 0 & R_a \end{bmatrix} \qquad [R_r] = \begin{bmatrix} R_A & 0 & 0 \\ 0 & R_A & 0 \\ 0 & 0 & R_A \end{bmatrix}$$

According to the relations (Equations 06), the equations of the asynchronous motor voltages are written as follows :

$$[\mathbf{u_{abc}}] = [\mathbf{R_s}][\mathbf{i_{abc}}] + [\mathbf{L_s}]\frac{\mathbf{d}}{\mathbf{dt}}[\mathbf{i_{abc}}] + \frac{\mathbf{d}}{\mathbf{dt}}([\mathbf{L_{sr}}][\mathbf{i_{ABC}}]) \quad (1)$$

$$[\mathbf{u_{ABC}}] = [\mathbf{R_r}][\mathbf{i_{ABC}}] + [\mathbf{L_r}]\frac{\mathbf{d}}{\mathbf{dt}}[\mathbf{i_{ABC}}] + \frac{\mathbf{d}}{\mathbf{dt}}([\mathbf{L_{sr}}][\mathbf{i_{abc}}]) \quad (2) \quad (08)$$

Given the dependence of $[L_{sr}]$with θ, the coefficients of the differential equations

(Equations 08) are variable and their analytical resolution is consequently very laborious, hence the introduction of the Park transformation [09] and [11], which will allow transforming the tension equations into constant coefficient differential equations.

The Park transformation consists in replacing three-phase windings with three equivalent windings, orthogonal to each other. Two of these windings (d and q) rotate, at speed ω= d/dt, in the plane defined by the three-phase windings (a, b and c) and the third (o) is perpendicular to this plane (see figure 13).

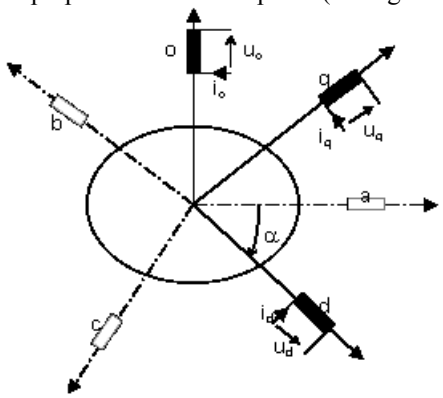

Figure 13:- Transformation of Park.

Three-phase and Park sizes are linked by the following relationships:

$$[\mathbf{i_{dqo}}] = [\mathbf{P}][\mathbf{i_{abc}}]$$

$$[\mathbf{u_{dqo}}] = [\mathbf{P}][\mathbf{u_{abc}}] \qquad \mathbf{(09)}$$

$$[\boldsymbol{\psi}_{\mathbf{dqo}}] = [\mathbf{P}][\boldsymbol{\psi}_{\mathbf{abc}}]$$

With :

$[i_{dqo}] = [i_d i_q i_o]^T$ $\qquad [u_{dqo}] = [u_d u_q u_o]^T$ $\qquad [\psi_{dqo}] = [\psi_d \psi_q \psi_o]^T$

$$[P] = \frac{2}{3}\begin{bmatrix} \cos\alpha & \cos(\alpha - \frac{2\pi}{3}) & \cos(\alpha + \frac{2\pi}{3}) \\ -\sin\alpha & -\sin(\alpha - \frac{2\pi}{3}) & -\sin(\alpha + \frac{2\pi}{3}) \\ \frac{1}{2} & \frac{1}{2} & \frac{1}{2} \end{bmatrix}$$

Since we use an asynchronous motor whose three-phase windings are star-connected with the neutral not connected, both at the stator and at the rotor, we always have : :

$i_o = i_a + i_b + i_c = 0$**(10)**

The instantaneous power in the three-phase windings is :

$$\mathbf{p(t) = u_a i_a + u_b i_b + u_c i_c} \qquad \textbf{(11)}$$

Applying Park's transformation to three-phase quantities (Equations 09), we obtain :

$$\mathbf{p(t) = \frac{3}{2}\left(u_d i_d + u_q i_q\right)} \qquad \textbf{(12)}$$

The magnetomotive force produced by windings d and q is projected as follows :

On the d axis :

$$\mathbf{f_{mm}(\alpha, t)_d = N_d i_d} \quad \textbf{(13)}$$

On the q axis :$\mathbf{f_{mm}(\alpha, t)_q = N_q i_q}$ (14)

Where N_d and N_q are the numbers of conductors of the equivalent windings d and q. These numbers can be chosen arbitrarily.

It can be seen that the magnetomotive forces produced by the three-phase windings and by the equivalent windings are equal, provided that and such that :

It can be seen that the magnetomotive forces produced by the three-phase windings and by the equivalent windings are equal, provided that N_d and N_q such that :

$$\frac{N_e}{N_d} = \frac{N_e}{N_q} = \frac{2}{3}$$

Where N_e is the number of effective conductors per phase, i.e. the number of conductors per phase multiplied by the winding coefficient.

We will transform the three-phase stator windings into equivalent d_s and q_s windings and the three-phase rotor windings into equivalent d_r and q_r windings (see figure 37).

We will transform the three-phase stator windings into equivalent d_s and q_s windings and the three-phase rotor windings into equivalent d_r and q_r windings (see figure 37).

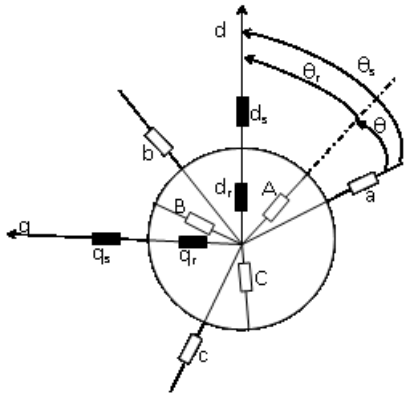

Figure 14:-Park transformation of stator and rotor values.

The transformation of the stator magnitudes is defined by:

$$\left[\mathbf{i_{dq}}\right]_{\mathbf{s}} = [\mathbf{P}]_{\mathbf{s}}[\mathbf{i_{abc}}] \quad (1)$$

$$\left[\mathbf{u_{dq}}\right]_{\mathbf{s}} = [\mathbf{P}]_{\mathbf{s}}[\mathbf{u_{abc}}] \quad (2) \quad \mathbf{(15)}$$

$$\left[\psi_{\mathbf{dq}}\right]_{\mathbf{s}} = [\mathbf{P}]_{\mathbf{s}}\left[\psi_{\mathbf{abc}}\right] \quad (3)$$

Where $$[P]_s = \frac{2}{3}\begin{bmatrix} \cos\theta_s & \cos(\theta_s - \frac{2\pi}{3}) & \cos(\theta_s + \frac{2\pi}{3}) \\ -\sin\theta_s & -\sin(\theta_s - \frac{2\pi}{3} & -\sin(\theta_s + \frac{2\pi}{3}) \end{bmatrix}$$

The transformation of the rotor values is defined by :

$$\left[\mathbf{i_{dq}}\right]_{\mathbf{r}} = [\mathbf{P}]_{\mathbf{r}}[\mathbf{i_{ABC}}]$$

$$\left[\mathbf{u_{dq}}\right]_{\mathbf{r}} = [\mathbf{P}]_{\mathbf{r}}[\mathbf{u_{ABC}}]\mathbf{(16)}$$

$$\left[\psi_{\mathbf{dq}}\right]_{\mathbf{r}} = [\mathbf{P}]_{\mathbf{r}}\left[\psi_{\mathbf{ABC}}\right]$$

Where

$$[P]_r = \frac{2}{3}\begin{bmatrix} \cos\theta_r & \cos(\theta_r - \frac{2\pi}{3}) & \cos(\theta_r + \frac{2\pi}{3}) \\ -\sin\theta_r & -\sin(\theta_r - \frac{2\pi}{3} & -\sin(\theta_r + \frac{2\pi}{3}) \end{bmatrix}$$

We have for the stator the flux equations in Park's frame :

$$\psi_{\mathbf{d_s}} = \mathbf{L_s i_{ds}} + \mathbf{L_{sr} i_{dr}}\mathbf{(17)}$$

$$\psi_{\mathbf{q_s}} = \mathbf{L_s i_{qs}} + \mathbf{L_{sr} i_{qr}}\mathbf{(18)}$$

Similar relationships are obtained for the rotor :

$$\psi_{\mathbf{d_r}} = \mathbf{L_r i_{dr}} + \mathbf{L_{sr} i_{ds}}\mathbf{(19)}$$

$$\psi_{\mathbf{q_r}} = \mathbf{L_r i_{qr}} + \mathbf{L_{sr} i_{qs}}\mathbf{(20)}$$

With : $$\mathbf{L_r = L_{AA} - L_{AB}}\mathbf{(21)}$$

In phase quantities, we have for the stator the voltage equations in Park's marker

$$\mathbf{u_{d_s}} = \mathbf{R_s i_{d_s}} + \frac{\mathbf{d\psi_{d_s}}}{\mathbf{dt}} - \omega_{\mathbf{s}}\psi_{\mathbf{q_s}}\mathbf{(22)}$$

$$\mathbf{u_{q_s}} = \mathbf{R_s i_{q_s}} + \frac{\mathbf{d\psi_{q_s}}}{\mathbf{dt}} + \omega_{\mathbf{s}}\psi_{\mathbf{d_s}}\mathbf{(23)}$$

By posing : $$\omega_{\mathbf{s}} = \frac{\mathbf{d\theta_s}}{\mathbf{dt}}\mathbf{(24)}$$

Similar relationships can be obtained for the rotor :

$$\mathbf{u_{d_r}} = \mathbf{R_r i_{d_r}} + \frac{\mathbf{d\psi_{d_r}}}{\mathbf{dt}} - \omega_{\mathbf{r}}\psi_{\mathbf{q_r}}\mathbf{(25)}$$

$$\mathbf{u_{q_r}} = \mathbf{R_r i_{q_r}} + \frac{\mathbf{d\psi_{q_r}}}{\mathbf{dt}} + \omega_{\mathbf{r}}\psi_{\mathbf{d_r}}\mathbf{(26)}$$

Where we posed :$\omega_r = \frac{d\theta_r}{dt}$ (27)

In general we will be in the case of squirrel-cage asynchronous motors (bars in short circuit) so $u_{d_r} = 0$ et $u_{q_r} = 0$.

There are 3 types of markers:

1. Stator-related marker :$\theta_s = 0$ therefore $\omega_s = 0$.
2. Rotor-related marker :$\theta_r = 0$ therefore $\omega_r = 0$.
3. Field related marker :$\theta_s = \theta_r + \theta$ therefore $\omega_s = \omega_r + \omega$.

The last mark is often used in the study of the power supply of variable frequency induction motors.

The instantaneous torque can be expressed as follows:

$$c_e = p\left(\psi_{d_s} i_{qs} - \psi_{q_s} i_{ds}\right) \quad (28)$$

It is possible to obtain other expressions of the torque by using the stator flux expressions [09], in this case we will have :

$$c_e = pL_{sr}\left(i_{dr} i_{qs} - i_{qr} i_{ds}\right) \quad (29)$$

Thus in equation 29 we have an expression of the instantaneous torque depending on the stator and rotor currents.

It is also possible to obtain a torque expression that depends on the rotor flux [09]. :

$$c_e = p\frac{L_{sr}}{L_r}\left(\psi_{d_r} i_{qs} - \psi_{q_r} i_{ds}\right) \quad (30)$$

Torque control can therefore be achieved by means of stator currents and rotor fluxes.

The Park model of the motor that will be developed using Simulink (see Figure 15) will use the above equations.

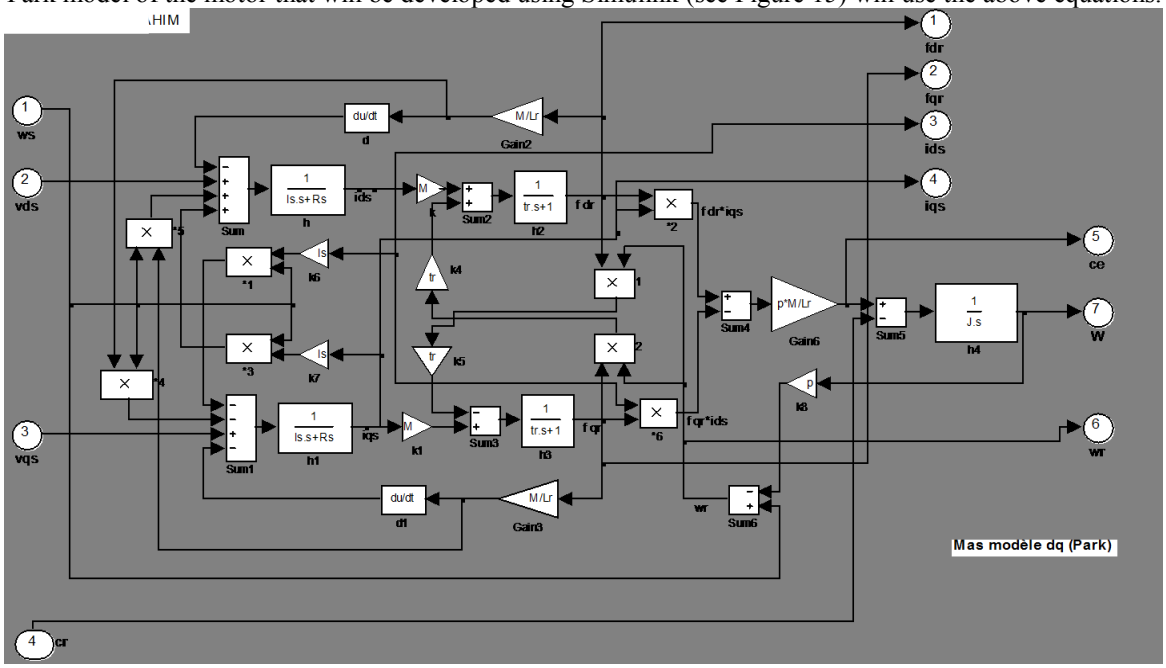

Figure 15:- Park model (d,q) of an asynchronous motor

The pump and hydraulic circuit model:

The centrifugal pump applies a load torque proportional to the square of the motor speed [01] [04] [20].

$$c_r = K_{ch}.\Omega^2 \quad (31)$$

With K_{ch} designates the proportionality constant of the pump.

Knowing the performance of a centrifugal pump (Q , H and P) for speed N , the similarity laws make it possible to determine the performance (Q' , H' and P') for a speed N' using the following relations : $Q' = Q\frac{N'}{N}$, $H' = \left(H\frac{N'}{N}\right)^2$, $P' = \left(P\frac{N'}{N}\right)^3$

where Q and Q' are the flow rates corresponding respectively to speed N and N'; H and H' are the total head corresponding respectively to speed N and N'; and P and P' are the motor powers corresponding respectively to speed N and N'.

The model that will be implemented will use the following equation :

$$\mathbf{H = a\omega^2 + b\omega Q - cQ^2}. \quad \textbf{(32)}$$

The hydraulic circuit (pipe and tank) is characterised by its HMT head.

For our model we will take a total manometric height HMT = 120 m. We have chosen the 4BHS4 48/40 pump manufactured by "POMPES MAROGER". This 4" submersible pump is equipped with a three-phase 380V (220V), 50 Hz motor with a power of 4 kW. The hydraulic characteristics of the pump are in the following table 2 :

Table 2:- Hydraulic characteristics of the pump.

Pump 4BHS	**kW**		**Q = Debit**						
		l/min	13	30	40	50	60	100	120
		M3/h	0,8	1,8	2,4	3,0	3,6	6	7,2
			H = HMT						
4BHS 48/40	4,0		-	253	241,1	227	210	109,4	-

To model this pump we first need to determine the values of the coefficients in equation 32. By substituting in this equation the value pairs of flow rate and head, we form 4 linear equations to be solved.
The Simulink model of the pump is shown in Figure 16 below. :

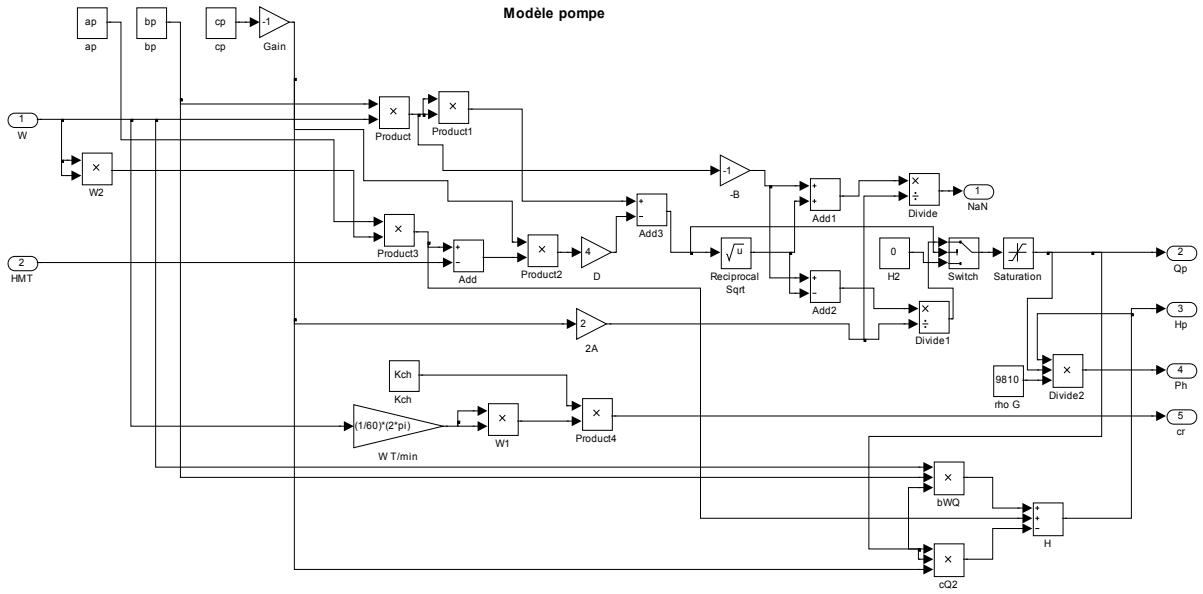

Figure 16:- Simulink model of the pump.

For the simulation we will consider that the quantity of water and its dynamic and static levels are sufficient to allow water pumping. On the other hand the head is taken equal to 120 m and is below the maximum limit height of our pump.

PWM and DTC control model:

PWM control model:

The inverter is controlled according to the natural PWM strategy. The switch control signals are determined by the intersection of a sinusoidal reference called "modulator" of frequency f_m with a triangular of high frequency f_p called "carrier" (see figure 17). Two indices [02] are therefore defined :

- Modulation index :$\mathbf{M} = \frac{\mathbf{f_p}}{\mathbf{f_m}}$ (32)

- Tension adjustment index r between 0 and 1 :$\mathbf{r} = \frac{\mathbf{V_{mod}}}{\mathbf{V_p}}$ (33)

For M ≥ 9 and for optimum cushioning, it is shown that :

The fundamental of the output voltage has as RMS value :

$\mathbf{V_m} = \frac{\mathbf{rU}}{\sqrt{2}}$ (34)

The harmonics are located around the central frequencies $k_1.M.f_m$ (k_1= 1, 2, 3,…).

For the case studied, we choose: r = 0.8 and M = 20

The switches of the inverter arms are controlled in a complementary way from the logic quantities (f_{ci}). The control signals are compared with the high-frequency triangular signal at any time. Switching of the switches will take place when we have an equality of the type :$V_{mod} = V_p$

During operation:

$$\text{Si} V_{mod} - V_p > 0 \quad \text{alors} f_{ci} = 1$$
$$\text{Si} V_{mod} - V_p \leq 0 \quad \text{alors} f_{ci} = 0$$

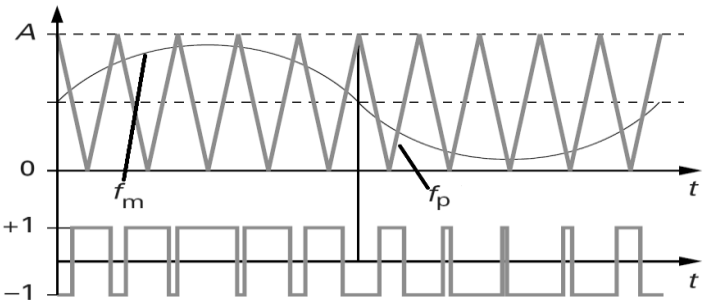

Figure 17:-Bipolar MLI (for one phase)

Figure 18 shows the Simulink model of the MLI control.

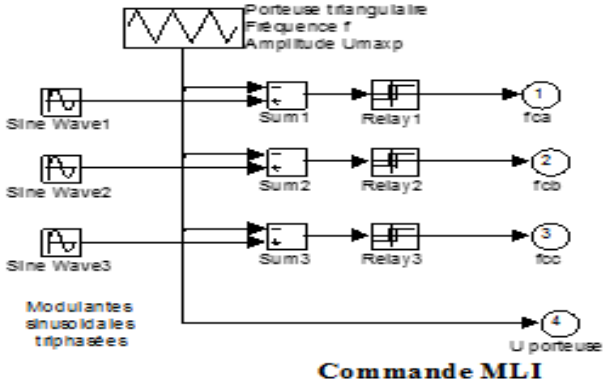

Figure 18:-Simulink model of the MLI control

DTC control model:
The control of our system is of the Direct Torque Control (DTC) type.

The methods of direct torque control of asynchronous machines appeared in the second half of the 1980s. They are intended to be competitive with conventional vector methods. They are based on pulse width modulation (PWM) power supply and a control strategy implementing an algorithm for decoupling the flux and motor torque by magnetic field orientation [22].

They consist of directly determining the control sequence applied to the switches of the voltage inverter. This choice is generally based on the use of hysteresis regulators whose function is to control the state of the system, in this case the amplitude of the stator flux and the electromagnetic torque.

The Direct Torque Control (DTC) of an asynchronous machine has outstanding dynamic performance and is robust against motor parameter deviations [23].

Direct Torque Control imposes switching commands on the arms at the times when it is required. The switching frequency is therefore variable depending on the desired operating point (Figure 19) [24].

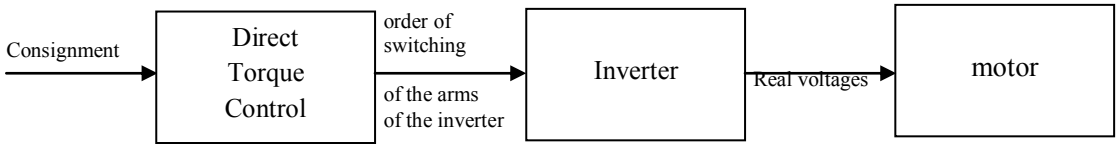

Figure 19:- Structure with direct torque control.

In a Concordia frame of reference (($\theta = 0$ in Park), the voltage vector is governed by the following differential equation) (equations 22, 23, 24 and 25 with $\theta = 0$
By posing :

$\bar{u}_s = u_{d_s} + j\,u_{q_s}$ $\quad\quad$ $\bar{u}_r = u_{d_r} + j\,u_{q_r}$

$\bar{i}_s = i_{d_s} + j\,i_{q_s}$ $\quad\quad$ $\bar{i}_r = i_{d_r} + j\,i_{q_r}$

$\bar{\psi}_s = \psi_{d_s} + j\,\psi_{q_s}$ $\quad\quad$ $\bar{\psi}_r = \psi_{d_r} + j\,\psi_{q_r}$

And with $\sigma = 1 - \frac{L_{sr}{}^2}{L_r L_s}$ Coefficient of dispersion
After calculation, the following equations can be found :

$$\bar{u}_s = R_s \bar{i}_s + \frac{d\bar{\psi}_s}{dt} \quad (35)$$

$$\frac{d\bar{\psi}_r}{dt} + \left(\frac{1}{\sigma\tau_r} - j\omega\right)\bar{\psi}_r = \frac{L_{sr}}{L_s}\frac{1}{\sigma\tau_r}\bar{\psi}_s \quad (36)$$

with $\tau_r = \frac{L_r}{R_r}$

These relationships show that :

1. It is possible to control the vector $\bar{\psi}_s$ from the vector $\bar{u}_s$, to $R_s\bar{i}_s$ the nearest voltage drop.
2. The flux $\bar{\psi}_r$ follows the variations of $\bar{\psi}_s$ with a time constant $\sigma\tau_r$, the rotor acts as a "time constant filter" between the flux $\bar{\psi}_s$ and $\bar{\psi}_r$.

$\bar{\psi}_r$ reaches in steady state the value : $\bar{\psi}_r = \frac{L_{sr}}{L_s}\frac{1}{1+j\,\omega\sigma\tau_r}\bar{\psi}_s$

While posing by $\gamma = \left(\widehat{\bar{\psi}_r, \bar{\psi}_s}\right) = \theta_s - \theta_r$, , the couple expresses themselves :

$$c_e = p\frac{L_{sr}}{\sigma L_s L_r}\psi_s\psi_r \sin\gamma \quad (37)$$

Le couple dépend de l'amplitude des deux vecteurs $\bar{\psi}_r$ et $\bar{\psi}_s$ and their relative position.

This equation shows that torque variations can be controlled from the angle γ thus the speed of rotation of the stator flux. If the angle γ increases the electromagnetic torque also increases, otherwise the torque decreases.

If one can perfectly control the flow $\bar{\psi}_s$ (from $\bar{u}_s$) in modulus and position, one can therefore control the amplitude and relative position of $\bar{\psi}_r$ and thus the torque. This is of course only possible if the control period T_c of the voltage $\bar{u}_s$ is such that $Tc << \sigma\tau_r$.

By solving equation 35 and neglecting the ohmic drop $R_s\bar{i}_s$ in front of the voltage $\bar{u}_s$ (this hypothesis is verified when the rotation speed is sufficiently high), the previous expression becomes:

$$\bar{\psi}_s(t) = \bar{\psi}_s(0) + \bar{u}_s t \quad (38)$$

It can then be seen that over an interval $[0,T_c]$, the end of the vector $\bar{\psi}_s$ moves on a straight line whose direction is given by the vector $\bar{u}_s$ selected during T_c .

This relationship is illustrated in Figure 20 with two choices of voltage vector: $\bar{u}_s = V_{s1}$ and $\bar{u}_s = V_{s4}$.

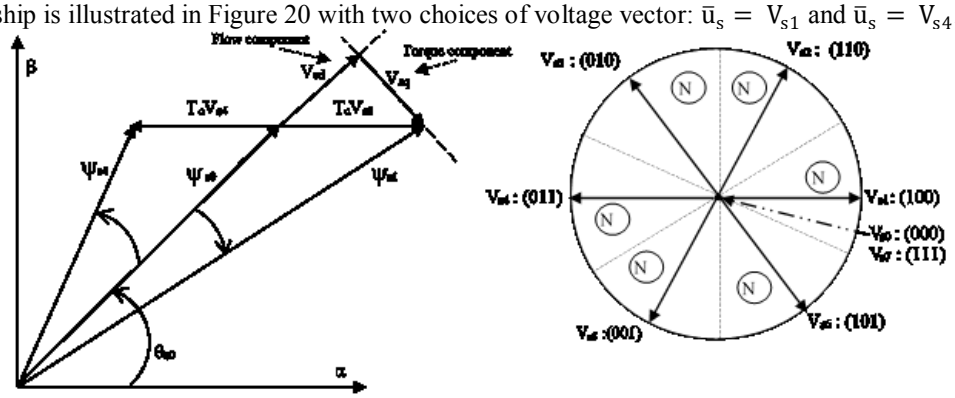

Figure 20:- Example of the evolution of the end of $\bar{\psi}_s$

The V_{s1} vector introduces an increase in the amplitude of the flow and a decrease in its speed. On the other hand, the V_{s4} vector decreases the amplitude of the flow but increases its speed.

It follows that the amplitude ψ_s of the stator flux vector $\bar{\psi}_s$ is controllable by the direct component V_{sd} of the voltage vector V_s , while its direction of rotation, and therefore its angle θ_s, is controllable by the quadrature component V_{sq}.

And, rotating the stator flux vector, leads to the creation of a torque. It is therefore possible to control both flux and torque directly by an appropriate choice of the raw voltage vector supplied to the inverter.

This direct torque control strategy for asynchronous machines is an alternative to scalar control and vector control. DTC control consists of controlling the stator flux amplitude and the electromagnetic torque. These quantities are estimated from the electrical stator quantities (current, voltage) without the use of a speed sensor and a pulse width modulation stage.

Table 3 illustrates the voltage vectors to be applied to increase or decrease the stator flux amplitude in each sector.

Table 3:- Flux control table.

Sector	ψ_s increase	ψ_s decrease
N1	V_{s1} , V_{s2} , V_{s6}	V_{s3} , V_{s4} , V_{s5}
N2	V_{s1} , V_{s2} , V_{s3}	V_{s4} , V_{s5} , V_{s6}
N3	V_{s2} , V_{s3} , V_{s4}	V_{s1} , V_{s5} , V_{s6}
N4	V_{s3} , V_{s4} , V_{s5}	V_{s1} , V_{s2} , V_{s6}
N5	V_{s4} , V_{s5} , V_{s6}	V_{s1} , V_{s2} , V_{s3}
N6	V_{s1} , V_{s5} , V_{s6}	V_{s2} , V_{s3} , V_{s4}

The torque will also be estimated using only measurable stator graders with the expression of equation 28: .: $c_e = p\left(\psi_{d_s} i_{qs} - \psi_{q_s} i_{ds}\right)$

If the flux amplitude ψ_s is kept within the hysteresis band around its reference value and the flux amplitude ψ_r is constant, equation 37, $c_e = p \frac{L_{sr}}{\sigma L_s L_r} \psi_s \psi_r \sin\gamma$, shows that the electromagnetic torque can be adjusted by adjusting the angle γ (angle between the stator and rotor fluxes).

The stator flux amplitude and the instantaneous torque are controlled separately. The control structure is summarised in Figure 21 below.

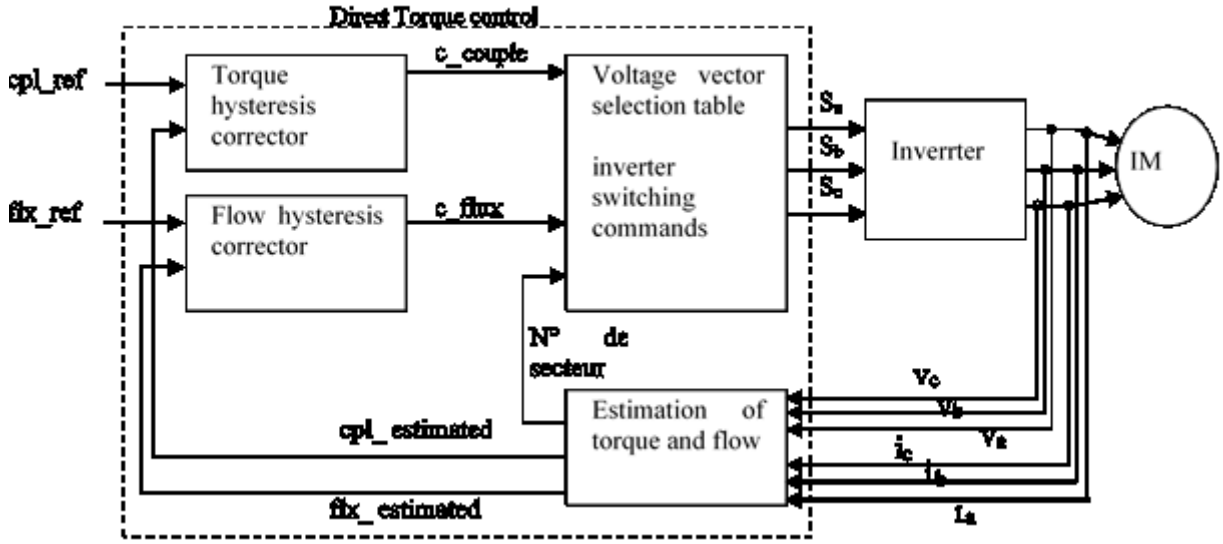

Figure 21:- Direct torque control structure.

Some Results:-

Result of the pumping system simulation with MPPT:

Table 7 and Figure 51 bring together the results of the simulation of the photovoltaic pumping system with maximum power point tracking.

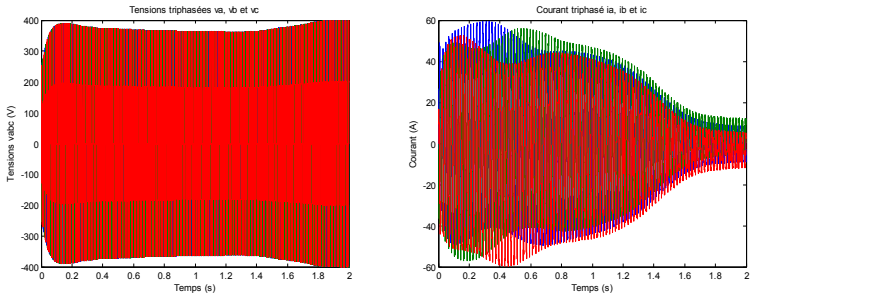

a) Three-phase voltage v_{abc} b) Three-phase current i_{abc}

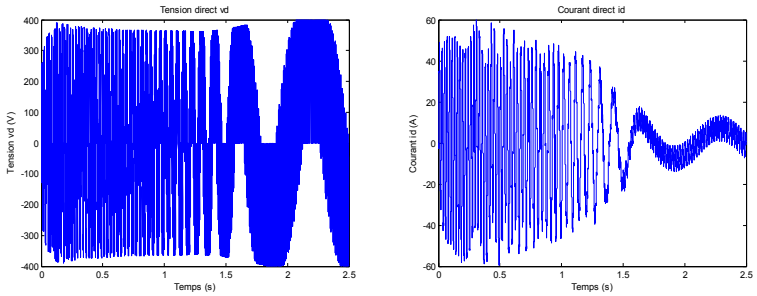

c) Voltage v_{ds} d) Currenti_{ds}

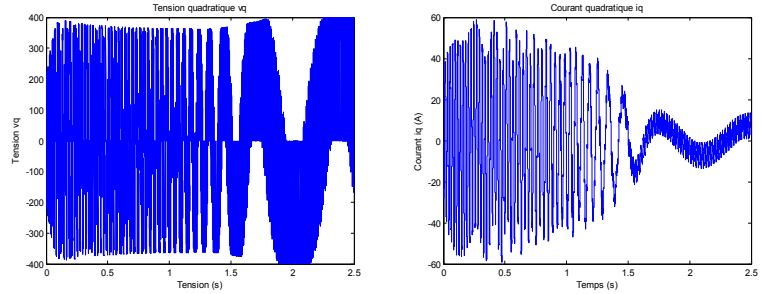

e) Voltage v_{qs} f) Currenti_{qs}

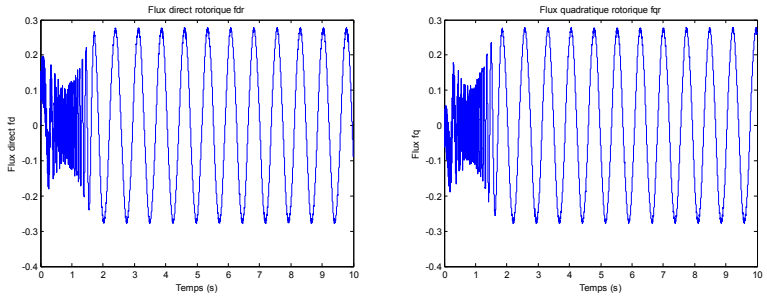

g) f_{dr} flow f)f_{qr} flow

Figures 22:- Results of the simulation of the dq model of an asynchronous motor under load (for 1000Wp).

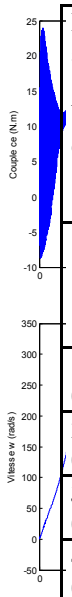

Irrad [Wc]	Maximum energy available on the Panels [Wh] in 10 sec.		Energy consumed on the Panels [Wh] in 10 sec		PV yield		Speed reached in 10 sec [RPM].		Quantity of water pumped [m^3]		Energy required to pump one m^3 of water [kWh/m^3].		Time taken to reach the HMT [s].		Maximum flow rate reached in 10 sec [m^3/h].	
	WITHOUT MPPT	WITH MPPT	WITHOUT MPPT	WITH MPPT	WITHOUT MPPT	WITH MPPT	WITHOUT MPPT	WITH MPPT	WITHOUT MPPT	WITH MPPT	WITHOUT MPPT	WITH MPPT	WITHOUT MPPT	WITH MPPT	WITHOUT MPPT	WITH MPPT
100	-	-	-	-	-	-	-	-	-	-	-	-	-	-	-	-
200	5.060	5.060	-	3.804	-	0.75	-	1557.40	-	-	-	-	-	-	-	-
300	8.167	8.167	-	7.017	-	0.86	-	2643.20	-	0.004886	-	1.436	-	5.42	-	4.817
400	12.160	12.160	-	10.620	-	0.87	-	2859.50	-	0.008989	-	1.181	-	3.52	-	5.645
500	14.450)	14.450	9.264	13.500	0.64	0.93	2 729.9	2899.90	0.008195	0.010960	1.130	1.232	3.70	2.63	5.158	5.793
600	17.590 m	17.590	9.578	17.110	0.54	0.93	2 739.8	2918.80	0.008520	0.012480	1.124	1.371	3.55	1.96	5.196	5.862
700	20.730	20.730	9.797	19.680	0.47	0.95	2 746.8	2918.80	0.008752	0.013050	1.119	1.508	3.44	1.69	5.223	5.862
800	23.840 r	23.840	9.973	22.720	0.42	0.95	2 752.2	2918.80	0.008929	0.013620	1.117	1.668	3.36	1.41	5.243	5.862
900	26.940 t	26.940	10.120	25.430	0.38	0.94	2 756.5	2918.80	0.009070	0.013830	1.116	1.839	3.29	1.31	5.260	5.862
1000	30.011	30.011	10.242	28.990	0.34	0.97	2 760.2	2 918.80	0.009188	0.014140	1.115	2.050	3.24	1.14	5.274	5.862

rque c_e i) speed w

Table 3:-Simulation results without and with MPPT.

Observations:-

With a MPPT we have a very consequent improvement in the efficiency of the energy absorbed by the system. This efficiency is of the order of 0.97 for an irradiation of 1000Wp, whereas it is only 0.34 without MPPT.

The pump reaches HMT in less time, 1.14 s for the system with MPPT, without MPPT it is 3.24 s. The pumping rate also improves; we have 5.863 m^3/H with MPPT and 5.273 without MPPT.

Simulation of the model incorporating DTC control:

The simulation of the optimised pumping system model (MPPT & DTC) gave us the results that we summarise in Tables 5 and 6 and in Figures 23.

For start-up, we first limited the torque set point to 20 N.m and then reduced it to 5 N.m after 1 second. This will keep the flow constant.

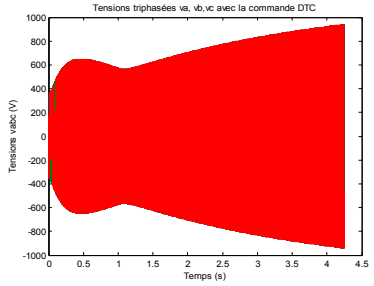

a) Three-phase voltage v_{abc}

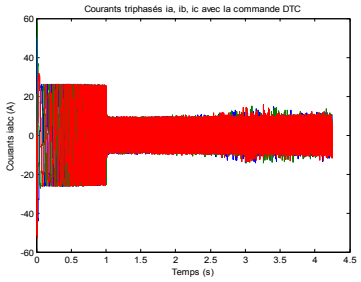

b) Three-phase current i_{abc}

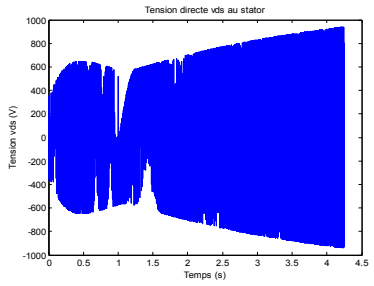

c) Voltage v_{ds}

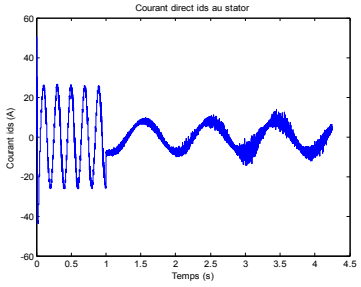

d) Currenti_{ds}

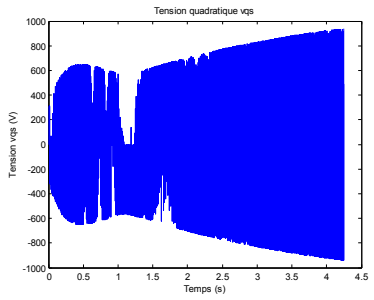

e) Voltage v_{qs}

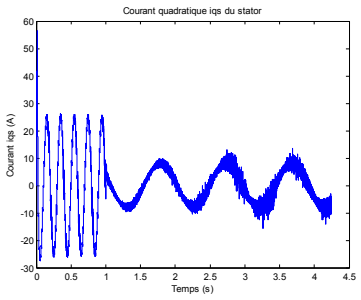

f) Currenti_{qs}

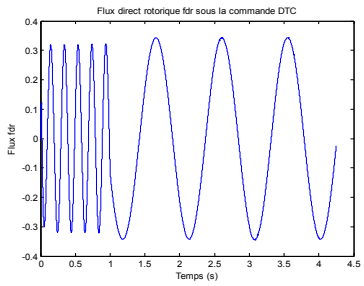

g) f_{dr} flow

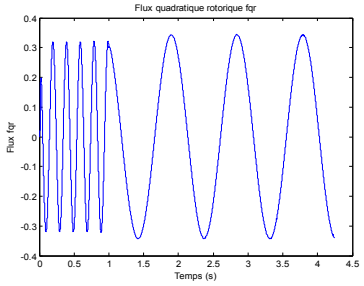

f)f_{qr} flow

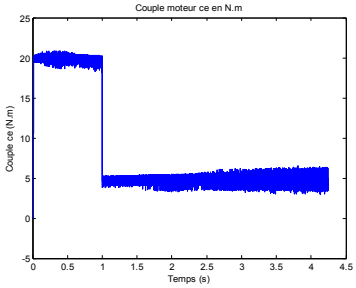

h) Motor torque c_e

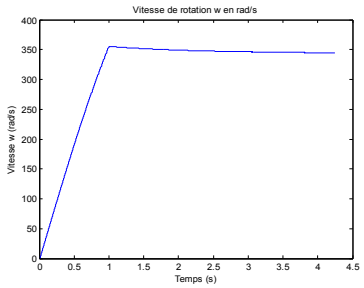

i) Rotational speed w

Figures 23:- Results of the simulation of the dq model of an asynchronous motor under load (for 1000Wp) optimised control (MPPT & DTC)

Observations the results in Table 5:
For an irradiation of 1000 Wp, we note on this first table an improvement on the efficiency of the consumed energy; it reaches 0.99 (compared to 0.97 with only the MPPT).

We have also increased with this order the quantity of water pumped, which rose to 0.0155 m3 (in 10s) against 0.0141 without DTC.

We are seeing a speed of up to 3317 rpm. This speed depends on the torque setting. It is adjusted according to the desired operating torque.

Observe the results in table 6:
A small improvement is obtained on the efficiency of the pump (the cubic meter of water will be pumped with less energy).

On the other hand, on the response time, the pump starts to deliver water as soon as 0.54 s (against 1.14 and 3.24 previously) and the maximum flow rate is reached in 0.85 s.

Table 5:- Results of the optimised pumping system model (MPPT & DTC).

Irradiation [Wp]	**Maximum energy available on the Panels [Wh] in 10 s**			**Energy consumed on the Panels [Wh]in 10 s**			**PV yield**			**Speed [RPM]achieved in 10 s**			**Quantity of water pumped [m^3] in 10 s pumping time**		
	WITHOUT MPPT	WITH MPPT	DTC	WITHOUT MPPT	WITH MPPT	DTC	WITHOUT MPPT	WITH MPPT	DTC	WITHOUT MPPT	WITH MPPT	DTC	WITHOUT MPPT	WITH MPPT	DTC
100	-	-		-	-		-	-		-	-		-	-	
200	-	5.060	5.060	-	3.804		-	0.75		-	-		-	-	
300	-	8.1	8.16	-	7.0		-	0.8		-			-	0.00	

		67	7		17			6						4886	
400	-	12.160	12.160	-	10.620		-	0.87		-			-	0.008989	
500	14.450	14.450	14.450	9.264	13.500		0.64	0.93					0.008195	0.010960	
600	17.590	18.360	18.360	9.578	17.110		0.54	0.93					0.008520	0.012480	
700	20.730	20.730	20.730	9.797	19.680		0.47	0.95					0.008752	0.013050	
800	23.840	23.840	23.840	9.973	22.720		0.42	0.95					0.008929	0.013620	
900	26.940	26.940	26.940	10.120	25.430		0.38	0.94					0.009070	0.013830	
1000	30.011	30.011	**30.011**	10.242	28.990	**29.763**	0.34	0.97	**0.99**	2918.80	2918.80	**3317.80**	0.009188	0.014140	**0.015586**

Table 6:- Results of the optimised pumping system model (MPPT & DTC) – continued.

Irradiation [Wc]	**Energy required to pump one m^3 of water [kWh/m3]**			**Time taken to reach the MTH [s]**			**Maximum flow rate reached in 10 s [m^3/h]**			**Quantity of water pumped [m^3] in 1 hour of pumping (estimated)**		
	WITHOUT MPPT	WITH MPPT	DTC	WITHOUT MPPT	WITH MPPT	DTC	WITHOUT MPPT	WITH MPPT	DTC	WITHOUT MPPT	WITH MPPT	DTC
100	-	-	-	-	-	-	-	-	-	-	-	-
200	-	-	-	-	-	-	-	-	-	-	-	-
300	-	1.436	-	-	-	-	-	-	-	-	1.758960	-
400	-	1.181	-	-	-	-	-	-	-	-	3.236040	-
500	1.130	1.232	-	3.70	-	-	5.158		-	2.950200	3.945600	-
600	1.124	1.371	-	3.55	-	-	5.196		-	3.067200	4.492800	-
700	1.119	1.508	-	3.44	-	-	5.223	5.862	-	3.150720	4.698000	-
800	1.117	1.668	-	3.36	-	-	5.243	5.862	-	3.214440	4.903200	-
900	1.116	1.839	-	3.29	-	-	5.260	5.862	-	3.265200	4.978800	-
1000	1.115	2.050	**1.910**	3.24	1.14	**0.54**	5.274	5.862	**6**	3.307680	5.090400	**5.610960**

Discussion:-

Based on the results of the simulation, we can see significant improvements at several levels of the photovoltaic pumping system.

Comparing the results given in Figures 22 and 23, it can be seen that with the system incorporating an MPPT :

A much more optimal power demand; overall we have a better yield for the energy absorbed in relation to the energy potentially available at the output of the photovoltaic panels. The yield is 0.97 as opposed to 0.33 (Table 3).

The stator voltages are of the order of 400V as opposed to 240V. The current peak at start-up is also much higher; it is about 60V compared to 45V without MPPT.

On the other hand, in steady state, the called stator current is less important with the MPPT; it has an amplitude of about 10A against 30A peak.

This result is due to the operating principle of the MPPT. It tends to bring the system back to the point of maximum operation of the photovoltaic panels. Hence the voltage and current values observed.

The steady state is reached in less time. Notwithstanding the best response in speed and torque, the MPPT has introduced a ripple of around 5 N.m on the torque.

We also observe a significant difference in the pump flow rate obtained. It is 5.862 m3/h compared to 5.274 m3/h.

The direct consequence of these results would be to revise the dimensioning of the solar panels downwards. Significant savings can be made in terms of investment in the installation of the photovoltaic group. The low stator current called is in favour of the operation of the Motor.

For the direct control of the DTC torque, introduced into the system, we can see the following from the simulation results. Note that in torque control, we have given an instruction of 20 N.m for 1s to accelerate the starting of the pump. This set point is reduced to 5 N.m afterwards.

This control strategy allows us to limit the stator current called at start-up to 50A as opposed to 60A in the previous case (figure 22.b and 23.b). This current will also be limited during the entire starting phase to a maximum current of around 25A. It will drop to 10A during steady state. The low current values, which are a consequence of the torque setpoint, will allow a much more acceptable motor load and operating constraints. Thus the motor's service life will be improved.

As the response time and the flow rate reach the set point, we are also observing progress. The rotation speed of 3317 T/min and the maximum pump flow rate of 6 m3/h are measured against 2918 T/min and 5.86m3/h respectively.

Apart from the stator current limit, we can notice a better torque response of the motor. In addition to the regulation obtained (in accordance with the given setpoint) we have obtained a significant reduction in the motor torque ripple rate. This ripple has adverse effects on the mechanical elements of the motor. Its reduction will certainly lead to more reliability in the pumping system.

Overall, significant improvements in terms of efficiency and behaviour under dynamic and steady state conditions have been achieved.

Conclusion:-

The important development in industry and in the modern way of life in recent years has made the use of energy compulsory. Electrical energy, in particular, has become the main factor in the development and even survival of our contemporary society. The limits of the reserves of non-renewable energy sources have led to interest in and search for other sources. To cover our energy needs, so-called renewable energy sources have become the essential substitutes for the future. One of the renewable energies that can meet this demand is solar energy, which is free and abundant in most parts of the world, and has proven to be an economical source, relative to other energies.

Unfortunately, however, the use of solar energy suffers from the high cost of photovoltaic cells and the low efficiency and intermittent power output due to fluctuating weather conditions. Therefore, any solar energy application system design should incorporate these unfavourable factors.

This paper is a contribution to the efficient and optimal use of photovoltaic energy in the water pumping sector. It has allowed us to propose and simulate viable and easy to implement solutions. The proposed optimisation of photovoltaic pumping systems is twofold.

The mismatch between the photovoltaic generator and its load results in a very low efficiency in the transfer and consumption of the available energy. At this level the improvement has consisted in setting up a maximum operating point tracker to improve this efficiency.

A second improvement is made at the level of the drive motor control. A DTC control is implemented to regulate the motor cut-off supplied to the pump.

The model and simulation of the optimised photovoltaic pumping system gave us satisfactory results. A significant improvement in the overall efficiency has been achieved. It went from 0.34 for the conventional system to 0.99 for the optimised system. Improvements have also been recorded in the pumping rate obtained.

It should be noted that this work is based on a simulation with constant sunlight and with fixed panels. In view of the satisfactory results obtained by the modelling, it will be advisable to complete this study by analysing the improvements that would be made by considering a full day of sunshine and by integrating a mechanical sun tracker on the system. An experimental study of the proposed pumping system will be an essential validation of our simulation.

References:-

1. Standard technique des systèmes de pompage photovoltaïque et de potabilisation, rapport (Standard Technique) financé par la Commission Européenne sous le contrat MEDA « Implementation of a PV Water Pumping Programme in Mediterranean Countries ». ref. ME8/AIDCO/2001/0132/SMAP-4.
2. MOUSSI, A. SAADI, Mai 2002. Etude comparative entre les techniques d'optimisation des systèmes de pompage photovoltaïque, LARHYSS Journal, N°.01, 12 Pages.
3. BETKA, A. MOUSSI, Juin 2003. Rendement maximise d'un moteur asynchrone alimente par une source photovoltaïque, LARHYSS Journal, ISSN 1112-3680, n° 02, pp. 151-162, © 2003 Laboratoire de Recherche en Hydraulique Souterraine et de Surface.
4. Jean-Claude MULLER, 2003.Électricité photovoltaïque – Principes, BE 8 578, Editions Techniques Ingénieurs.
5. MOHAMED A., 2007. Optimisation de l'ensemble onduleur, moteur et pompe branche sur un générateur photovoltaïque, Thèse présentée pour l'obtention du diplôme de Docteur d'Etat Spécialité : Electronique,UNIVERSITE MENTOURI DE CONSTANTINE FACULTE DES SCIENCES DE L'INGENIEUR DEPARTEMENT ELECTRONIQUE, ALGERIE.127 Pages,
6. BELHADJ M., 2008. Modélisation d'un système de captage photovoltaïque autonome, Mémoire de Magister option : Microélectronique –Photovoltaïque, Centre Universitaire De Bechar Institut des Sciences Exactes, ALGERIE.95 Pages.
7. Henri FOCH et Al., 2003. Conversion continu-continu - Hacheurs, D 3 160, Editions Techniques Ingénieurs.
8. Henri FOCH et Al., 2003.Onduleurs de tension - Mise en œuvre, D 3 177, Editions Techniques Ingénieurs.
9. LOUAZENE M. L., 2008, Etude technico-économique d'un système de pompage photovoltaïque sur le site de Ouargla, MAGISTER en électrotechnique Option : Maîtrise d'Energie, Faculté des Sciences de l'Ingénieur Département d'Electrotechnique, UNIVERSITE EL HADJ LAKHDAR – BATNA ALGERIE.101 Pages.
10. SAGNA A., 2008. Régulation de la vitesse d'un moteur asynchrone par commande vectorielle, PROJET DE FIN D'ETUDE INGENIEUR DE CONCEPTION, Département Génie Mécanique, Ecole Supérieure Polytechnique de THIES, UNIVERSITE CHEIKH ANTA DIOP DE DAKAR, 87 Pages.
11. KSB Aktiengesellschaft, 2005. Détermination des pompes centrifuges, Allemagne.
12. BIMAL K. BOSE, 2002. Modern Power Electronics and AC Drives, ISBN 0-13-016743-6, Prentice Hall PTR.
13. D.Saheb-Koussa, M.Haddadi, Modélisation d'un générateurphotovoltaïque dans l'environnement « Matlab », 03-04 November 2007, 4th International Conference on Computer Integrated Manufacturing CIP'2007,
14. GOETZBERGER, V.U. HOFFMANN, 2005. Photovoltaic solar energy generation, Springer Series in optical sciences, ISBN 3-540-23676-7, Springer, PAGES 239.
15. O.AMRANI, D.REKIOUA, . Etude et identification des différents modèles électriques photovoltaïques, Département d'électrotechnique, Université de Bejaia, (Algérie).
16. MUSTAPHA B., Modélisation et simulation d'un système de pompage photovoltaïque, MEMOIRE en vue de l'obtention du diplôme de magister spécialité : électronique ; option : systèmes photovoltaïques, FACULTE DE

GENIE ÉLECTRIQUE, DEPARTEMENT D'ÉLECTRONIQUE, UNIVERSITE DES SCIENCES ET DE LA TECHNOLOGIE D'ORAN MOHAMED BOUDIAF, 108 Pages.
17. O. GERGAUD, B. MULTON, H. BEN AHMED, august 2002. Analysis and Experimental Validation of Various Photovoltaic System Models, 7th International ELECTRIMACS Congress, Montréal.
18. HOUSSAMO, M. SECHILARIU, F. LOCMENT, G. FRIEDRICH, 2010. Identification of Photovoltaic Array Model Parameters. Modelling and Experimental Verification, International Conference on Renewable Energies and Power Quality (ICREPQ'10) Granada (Spain), 23th to 25th March, 2010.
19. MARCELO G. V., JONAS R. G., ERNESTO R. F., 2009. Comprehensive Approach to Modeling and Simulation of Photovoltaic Arrays, IEEE TRANSACTIONS ON POWER ELECTRONICS, VOL. 24, NO. 5, MAY 2009.
20. M. G. VILLALVA, J. R. GAZOLI, E. RUPPERT F., 2009. Modeling and circuit-based simulation of photovoltaic arrays, Brazilian Journal of Power Electronicc, 2009, Vol. 14, no. 1, pp. 35-45, ISSN 1414-8862.
21. M.N. Mansouri, N. Ghanmi et M.F. Mimouni, 2008. Commande et analyse des performances d'une station de pompage photovoltaïque fonctionnant en régime optimal, Revue des Energies Renouvelables Vol. 11 N°1 , 1 – 17.
22. LOKRITI, Y. ZIDANI, S. DOUBABI, 2010. Comparaison des performances des regulateurs pi et ip appliques pour la commande vectorielle a flux rotorique oriente d'une machine asynchrone, 8e Conférence Internationale de Modélisation et Simulation - MOSIM'10 - 10 au 12 mai 2010 - Hammamet – Tunisie « Evaluation et optimisation des systèmes innovants de production de biens et de services » .
23. ELBACHA, M. T.LAMCHICH , M. CHERKAOUI , Contrôle direct de couple d'une machine asynchrone système de régulation de vitesse avec anti-emballement,. Faculté des sciences Sémlalia, Université Cadi-Ayyad, Marrakech.
24. Cours élaboré par Hasnaoui Othman, 1995.Commandes des machines – Tizi Ouzou.
25. Cours Hasnaoui Othman, 1995. Optimisation de la commande rapprochée du moteur. – Tizi Ouzou.